Received: 23 January 2021 | Revised: 16 February 2021 | Accepted: 18 February 2021

DOI: 10.1002/pro.4055

PROTEIN STRUCTURE REPORTS

Structural characterization of the self-association domain of swallow

Nikolaus M. Loening[1] | **Elisar Barbar**[2]

[1]Department of Chemistry, Lewis & Clark College, Portland, Oregon

[2]Department of Biochemistry and Biophysics, Oregon State University, Corvallis, Oregon

Correspondence
Nikolaus M. Loening, Department of Chemistry MSC 55, Lewis & Clark College, 615 S Palatine Hill Road, Portland, OR 97219, USA.
Email: loening@lclark.edu

Funding information
Division of Molecular and Cellular Biosciences, Grant/Award Numbers: Award 1617019, Award 1617019 Amendment 1; FP7 Research infrastructures, Grant/Award Number: Project 261863 Bio-NMR; M.J. Murdock Charitable Trust, Grant/Award Number: 2014162; National Institutes of Health, Grant/Award Number: 1S10OD018518

Abstract

Swallow, a 62 kDa multidomain protein, is required for the proper localization of several mRNAs involved in the development of Drosophila oocytes. The dimerization of Swallow depends on a 71-residue self-association domain in the center of the protein sequence, and is significantly stabilized by a binding interaction with dynein light chain (LC8). Here, we detail the use of solution-state nuclear magnetic resonance spectroscopy to characterize the structure of this self-association domain, thereby establishing that this domain forms a parallel coiled-coil and providing insight into how the stability of the dimerization interaction is regulated.

KEYWORDS

coiled-coil, dimer, protein structure, self-association domain, solution-state NMR spectroscopy

1 | INTRODUCTION

Swallow is a multidomain Drosophila protein (UniProt[1] Entry P40688) that is required for the proper localization of several mRNAs that are involved in oogenesis, such as *bicoid* mRNA[2] and *huli-tai shao*-adducin-like mRNA.[3] Sequence analysis and biophysical measurements[4,5] strongly imply that Swallow has the domain structure shown in Figure 1(a), in which the mostly disordered N- and C-terminal regions flank a central self-association domain consisting of residues 205–275. Upon dimerization, this self-association domain is predicted to form a dimeric α-helical parallel coiled-coil with the heptad repeat pattern shown in Figure 1(c). Our previous studies of this system[4,5] suggest the model shown in Figure 1(b) in which, on its own, Swallow's propensity for self-association is relatively weak. The dimeric form of Swallow is greatly stabilized by the binding of dynein light chain LC8 (DYNLL1), a highly-conserved homodimeric hub protein,[6–8] at a site that is close to, but separate from, Swallow's self-association domain.

At physiological temperatures and concentrations, Swallow's dimerization interaction is relatively weak with a dissociation constant of 4 μM at 20°C, and is prone to aggregation at higher concentrations.[4] Consequently, for the purpose of structurally characterizing the dimeric form of this self-association domain, which is stabilized by LC8 binding, we focused on a construct of residues 205–275 (Swa_{DIMER}) that incorporates two key mutations that allow it to form stable and soluble dimers in the absence of LC8.[5] As shown in Figure 1, an arginine at position 224 was replaced with a glutamate (R224E) to minimize electrostatic repulsion with lysine 219, and a lysine at position 244 was replaced with an isoleucine (K244I) to remove a charged residue from the coiled-coil's hydrophobic interface. These two substitutions were sufficient to promote formation of a stable dimer at temperatures of up to 60°C.[5] In addition to these two

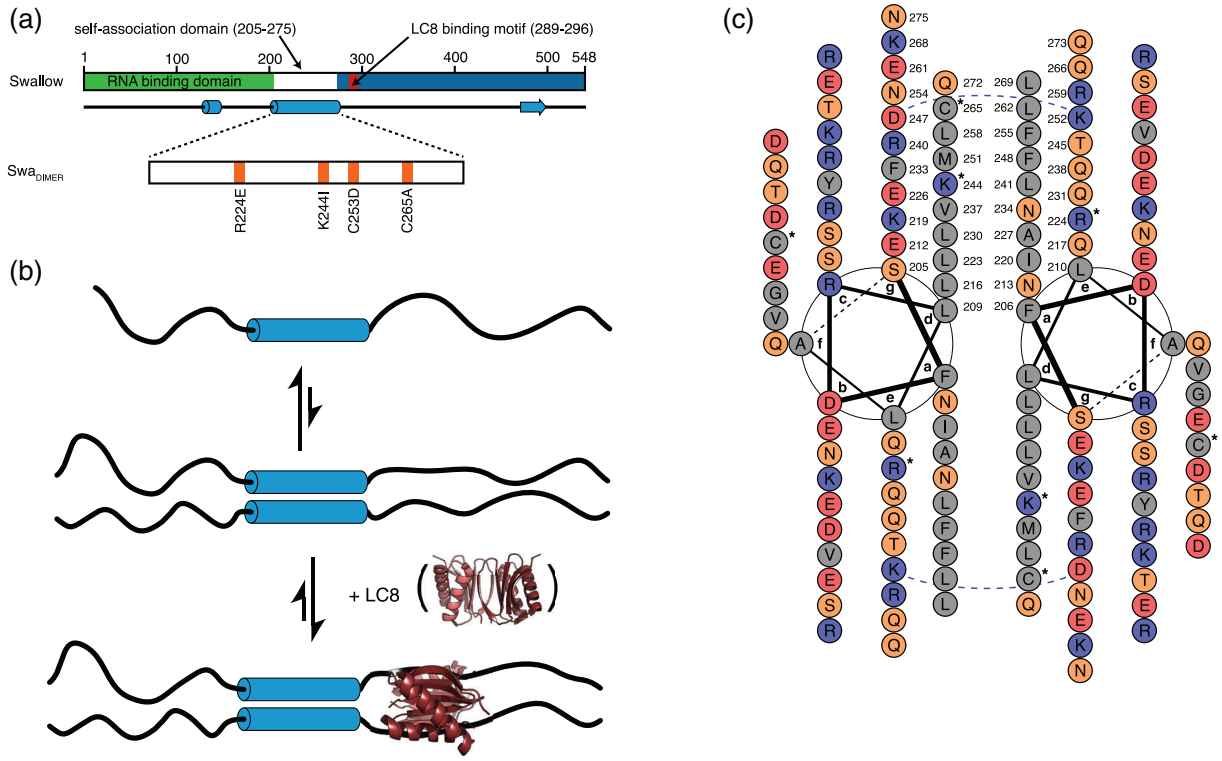

FIGURE 1 Schematic domain structure of Swallow, model of its interaction with LC8, and helical wheel diagram for the self-association domain. (a) The self-association domain of Swallow (residues 205–275) forms a coiled-coil upon dimerization, whereas the remainder of the protein is predicted to be mostly intrinsically disordered (solid line), except for short α-helical (barrel) and β-sheet (arrow) regions. For studying the structure of the self-association domain, a construct with stabilizing mutations (Swa$_{DIMER}$) was used. (b) Previous work with Swallow indicates that the dimerization interaction is relatively weak, resulting in an equilibrium between monomeric and dimeric forms in solution that is almost entirely shifted to the dimeric form upon binding by LC8.[4,5] The LC8 homodimer (Protein Data Bank entry 3E2B) was rendered using PyMOL.[37] (c) Helical wheel diagram for the predicted coiled-coil region of Swallow (residues 205–275) generated using DrawCoil 1.0.[38] The hydrophobic residues at the a and d positions of the heptad repeat form the interaction surface of the dimer. Colors in the diagram indicate amino acids types: hydrophobic (grey), basic (blue), acidic (red), hydrophilic neutral (orange). Dashed blue lines indicate the location of hydrogen bonds that are predicated to stabilize the coiled-coil structure. Locations of the mutations (R224E, K244I, C253D, and C265A) in the Swa$_{DIMER}$ construct are indicated by asterisks (*)

stabilizing mutations, two further mutations to remove cysteines (C253D, C265A) were introduced to prevent aggregation due to disulfide bond formation, thereby easing sample preparation and structural characterization. Although these mutations result in a stabilized dimer, the structure described in this paper differs from an "ideal" coiled-coil and hints at how evolution might have shaped the stability of the coiled-coil in Swallow such that binding with LC8 at a site ~15 residues away from the self-association domain can easily perturb Swallow's monomer-dimer equilibrium.

Previous examples of coiled-coils studied using nuclear magnetic resonance (NMR) spectroscopy include monomers that form hairpins (Protein Data Bank[9] entries 2K48[10] and 2KE4[11]), parallel homodimers (1JUN,[12,13] 2GD7,[14] 5IEW,[15] 6N2M[16]), antiparallel homodimers (1HF9,[17] 2LW9,[18] 2N9B,[19] and 6E4H[20]), heterodimers (2A93[21]), homodimers that form four-helix bundles (2MAJ[22]), homotrimers (2FXP,[23] 2KP8,[24] and 2N64[25]), and even computationally designed heterodimeric four-helix bundles (6DMP[26]). Swa$_{DIMER}$ is, to our knowledge, the longest coiled-coil structure determined by NMR spectroscopy to date, albeit only slightly longer than the coiled-coil structures in some previous studies.[14,25]

2 | RESULTS

2.1 | Chemical shift assignments

We were able to completely assign the ^{1}H, ^{13}C, and ^{15}N chemical shifts of all backbone and sidechain resonances for Swa$_{DIMER}$ with the exception of amino, hydroxyl, carboxyl, and guanidinium functional groups (due to fast exchange with the solvent), and phenylalanine/tyrosine γ-carbons and tyrosine ζ-carbons. In doing so, we corrected

some mistakes in the previous chemical shift assignments.[5] Only a single set of peaks were observed in the NMR spectra, which is consistent both with the expected structure of a parallel coiled-coil dimer with C_2 symmetry and with the presence of a single oligomeric form. Analysis of the secondary chemical shifts as a function of heptad position is provided in the Supplementary Material (see Figure S1).

2.2 | Calculation of the Swa_{DIMER} structure

Coiled-coil structures tend to have NMR spectra with limited chemical shift dispersion for amide resonances, leading to ^{1}H-^{15}N correlation spectra (Figure S2A) that resemble those for intrinsically disordered proteins. As a result of the small de-gree of chemical shift dispersion, chemical-shift matching of the peaks in the NOESY spectra resulted in NOE restraints that were highly ambiguous. This ambiguity was further increased because many of these peaks could be due to intra- or interchain interactions. Due to this high ambiguity, initial attempts to calculate the structure using ARIA[27] resulted in the occasional appearance some "hair-pin" structures in the ensemble due to erroneous long-range restraints biasing the initial rounds of the structure calculation. To promote convergence without manually assigning the majority of the NOE peaks, we used a low-energy structure from a

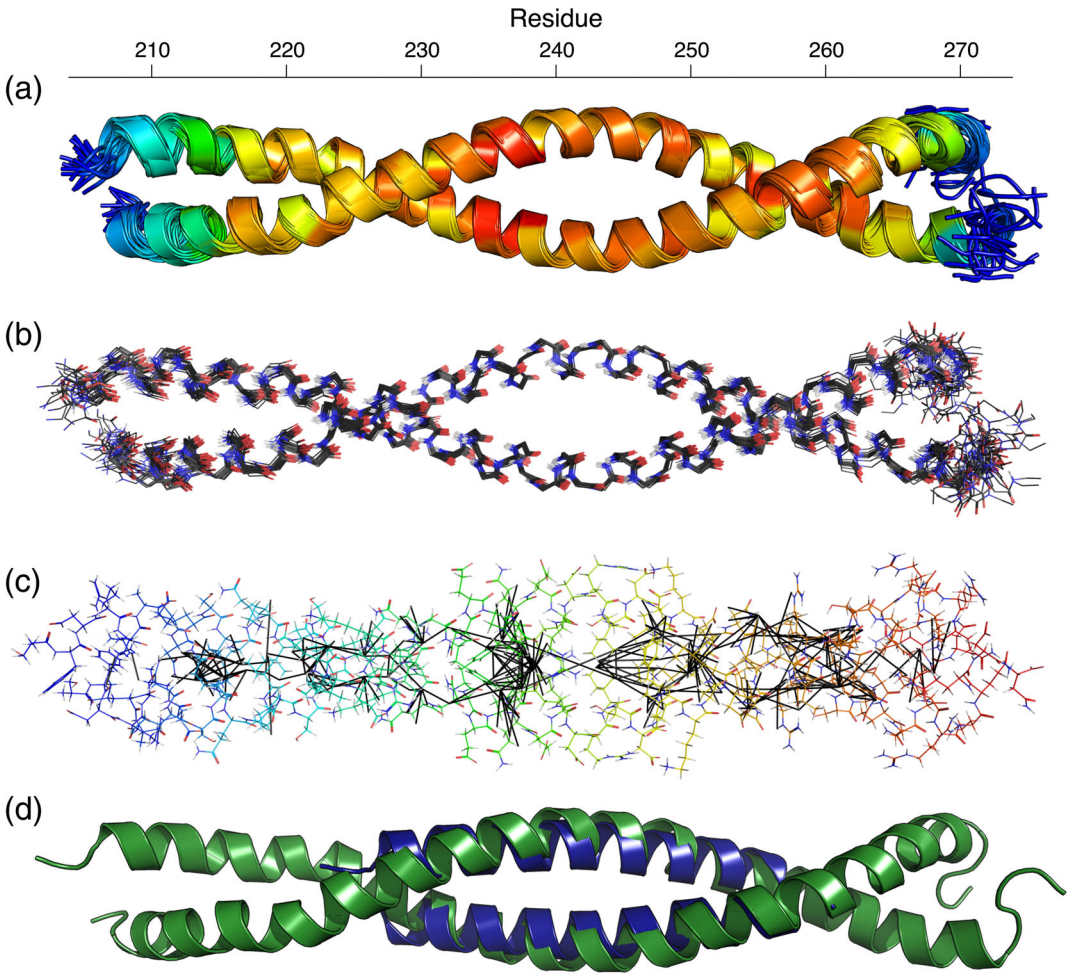

FIGURE 2 (a) Structural ensemble for Swa_{DIMER}. Cartoon representation of the water-refined Swa_{DIMER} structural ensemble calculated using a combination of NOE restraints, residual dipolar couplings, and chemical shift-based torsion angle restraints. The structure is oriented with the N-terminus (residue 205) on the left and the C-terminus (residue 275) on the right; an approximate scale is provided at the top of the figure. Colors represent the R_2/R_1 values from Figure S3F, with the minimum value colored blue and the maximum value colored red. (b) Wireframe representation of the Swa_{DIMER} structural ensemble showing only the backbone atoms. Carbon, nitrogen, oxygen, and hydrogen atoms are colored black, blue, red, and white, respectively. (c) Wireframe representation of the lowest-energy structure in the Swa_{DIMER} ensemble with black lines indicating the location of the intermolecular NOEs used in the structure calculation to constrain the dimer structure. (d) Overlay of the lowest-energy structure from the Swa_{DIMER} structural ensemble (in green) with the leucine zipper region of GCN4 (in blue, PDB 5IEW[15]) illustrating the "bulge" in the center of the Swa_{DIMER} coiled-coil

TABLE 1 Structural statistics for the Swa_{DIMER} ensemble

Physical parameters	
Number of residues	71 × 2 = 142
Average molecular weight (unlabeled, Da)	8544.4 × 2 = 17,088.8
Structural restraints	
NOE-derived distance restraints (ARIA cycle 8)	
Intraresidue ($\|i–j\| = 0$)	566
Sequential ($\|i–j\| = 1$)	295
Short ($2 \leq \|i–j\| \leq 3$)	223
Medium ($4 \leq \|i–j\| \leq 5$)	110
Long ($\|i–j\| > 5$)	0
Interchain	110
Ambiguous	1302
Total	2699
Dihedral constraints	
Phi	64 × 2 = 128
Psi	64 × 2 = 128
Residual dipolar couplings (RDC)	
$^1D_{HN}$	43 × 2 = 86
Statistics for accepted structures	
Accepted structures	20 of 100
Mean CNS energy terms	
E total (kcal mol^{-1})	−4,260 (±140)
E van der Waals (kcal mol^{-1})	−312 (±16)
E NOE distance restraints (kcal mol^{-1})	820 (±10)
E dihedral angle restraints (kcal mol^{-1})	3.2 (±1.8)
E RDC restraints (kcal mol^{-1})	4.0 (±1.0)
Restraint violations	
NOE > 1.0 Å, > 0.5 Å (average # per structure)	0, 21 (±2)
Dihedral >5° (average # per structure)	0.1 (±0.4)
$^1D_{HN}$ RDC > 1 Hz, > 0.5 Hz (average # per structure)	0, 2 (±2)
RMS deviations from the ideal geometry used within CNS	
Bond lengths (Å)	4.19×10^{-3} ($\pm 8 \times 10^{-5}$)
Bond angles (°)	0.532 (±0.015)
Improper angles (°)	1.25 (±0.08)
Ramachandran statistics (PROCHECK 3.5.4[35])	
Most favored (%)	96 (±3)
Additionally allowed (%)	4 (±3)
Generously allowed (%)	0
Disallowed (%)	0
Average atomic RMS deviations from average structure[a]	
N, C_α, C, and O atoms (all residues, Å)	0.91 (±0.17)
All heavy atoms (all residues, Å)	1.38 (±0.16)
N, C_α, C, and O atoms (for residues 207–271, Å)	0.47 (±0.14)
All heavy atoms (for residues 207–271, Å)	0.98 (±0.15)

(Continues)

TABLE 1 (Continued)

Physical parameters	
MolProbity analyses (v3.19[36])	
Clashscore	20.0 (±1.2)
Clashscore percentile (%)	33 (±3)
Clashscore Z-score	−0.41 (±0.09)

[a]Two sets of atomic RMS deviations are provided. The first set is for the full-length sequence (residues 205–275), whereas the second set is calculated including only residues for which the circular order parameters (cop) for both φ and ψ are ≥0.9 (residues 207–271).

prior calculation, rather than a structure with randomized torsion angles, as the initial structure in the ARIA protocol. This allowed all of the NOEs to be properly assigned by ARIA, and resulted in a contact map that shows the expected short- and medium-range NOE contacts and a complete absence of long-range contacts (Figure S2B). Intermolecular NOE restraints were gathered using a $^{13}C/^{15}N$-filtered NOESY experiment with a sample containing a 1:1 mixture of isotopically-labeled and unlabeled Swa_{DIMER} (Figure S2C). This resulted in almost 100 interchain NOE restraints that were distributed across most of the dimer interface (Figure 2(c)).

2.3 | Analysis of the Swa_{DIMER} structure

The structure calculation resulted in a well-converged ensemble (Figure 2(a),(b), Table 1) that shows an almost completely coiled-coil structure with only a small amount of fraying at the C-terminus. This structure is consistent with coiled-coil predictions, measurements of $^{1}D_{HN}$ residual dipolar coupling (RDC) values, and measurements of ^{15}N relaxation rates for Swa_{DIMER} (Figure S3). The Swa_{DIMER} structure shows looser coiled-coil packing in the center of the structure at a position that matched the K244I mutation that was needed to stabilize the dimer structure, resulting in a bulge that other coiled-coils lack (Figure 2(d)).

Coiled-coil structure can be identified by the presence of a characteristic "knobs-into-holes" side-chain packing first detailed over 50 years ago,[28] in which the "knob" formed by the sidechain of an amino acid in one helix packs into a "hole" made from four residues on the opposite helix. Using SOCKET[29] with a packing distance cutoff of 7.0 Å, we found 12 knobs-into-holes interactions for each chain of Swa_{DIMER}, with the knobs distributed relatively evenly along the chain (residues 213, 216, 220, 223, 227, 230, 248, 251, 255, 258, 262, and 265 were identified as knobs). There is a gap in the appearance of knobs between residues 230 and 248, consistent with reduced packing in this "bulge" region.

We also analyzed the Swa_{DIMER} structure using the CCCP (Coiled-Coil Crick Parameterization) tool,[30] which fits α-helices to the Crick parameterization for ideal coiled-coils.[28] This analysis shows that the entire length of Swa_{DIMER} is not well-described by a single set of coiled-coil parameters due to the bulge in the middle of the structure (for further details, see the Supplementary Material and Table S1).

3 | DISCUSSION

The reduced packing ("bulge") in the middle of the Swa_{DIMER} structure (approximately residues 235–250) suggests the possibility that, in the wild-type sequence, it is the center of the self-association domain that destabilizes the coiled-coil and results in the observed monomer-dimer equilibrium.[5] We hypothesize that this locus of instability is what drives the monomer-dimer equilibrium of Swallow so that the formation of the active, dimeric form can be facilely regulated by interacting with the hub protein LC8, a binding partner that regulates the dimerization of a wide variety of proteins in vivo.[6–8] This form of regulation has been previously observed, for example, in the tetrameric coiled-coil multimerization domain of RNA virus phosphoprotein where a locus of instability was correlated with viral activity.[31] Interestingly, the region of Swa_{DIMER} with the bulge does not have noticeably different ^{15}N relaxation properties than more tightly-packed regions, indicating a lack of additional dynamics on the pico- and nanosecond time scale. This can be rationalized by the fact that the bulge region, like the rest of the protein, is composed of relatively rigid α-helices. Consequently, we believe it likely that processes on much slower time scales are responsible for the monomer-dimer interconversion in the wild-type protein.

The amide peaks (Figure S2A) for Swa_{DIMER} are broader than what would typically be expected for a ~ 17 kDa protein complex. This is attributable to anisotropic tumbling of the long, axially-symmetric Swa_{DIMER} structure, which results in a correlation time for

tumbling about the long axis (i.e., the symmetry axis) that is much shorter than the rotational correlation times for tumbling about perpendicular axes. As has been noted previously,[13] the N—H bond vectors for the backbone amides in coiled-coils are nearly parallel to the long axis (Figure 2b), so the ^{15}N relaxation rates are insensitive to tumbling about this axis and any correlation times estimated from these relaxation rates reflect the slower tumbling about the axes perpendicular to the long axis.

The unfavorable ^{15}N relaxation rates for amides in coiled-coils such as Swa_{DIMER} (Figure S3E) sets a limit to the size of coiled-coil that can be studied by NMR. In the case of Swa_{DIMER}, the spectra were still interpretable due to the use of high relatively high temperatures (40°C) and high magnet fields (which maximize the TROSY effect). We believe that Swa_{DIMER} is close to the limit of what can reasonably be studied by NMR for regular (protonated) samples. To tackle longer coiled-coil systems, deuteration of non-amide protons might further improve linewidths, especially if TROSY-based experiments are used. However, this would be at the expense of the number of NOEs (and, in particular, intermolecular NOEs) that can be measured for structure determination. Still larger coiled-coils may be achievable using selective methyl-labeling strategies and methyl-TROSY experiments, but would be complicated by the lack of chemical shift dispersion for the methyl peaks of coiled-coil proteins.

4 | CONCLUSION

Our solution-state NMR structure confirms sequence-based predictions that the self-association domain of Swallow forms a symmetrical homodimeric coiled-coil. Interestingly, the center of this domain deviates from the ideal packing for a coiled-coil, resulting in a bulge. As the location of this bulge matches the position of the main mutation (K244I) used to stabilize the dimeric form, we hypothesize that this is the site of structural instability that drives the monomer-dimer equilibrium for wild-type Swallow. Our structure of Swa_{DIMER} is, at present, the longest coiled-coil structurally characterized by solution-state NMR spectroscopy, and is likely close to the practical limit of what can accomplish using NMR without resorting to deuteration and methyl-labeling strategies.

5 | MATERIALS AND METHODS

Isotopically-labeled (^{15}N and ^{15}N/^{13}C) samples of Swa_{DIMER} were prepared as previously described.[5] A brief summary of the sample preparation is provided in the Supplementary Material.

All NMR spectra were acquired using a sample temperature of 40°C on NMR spectrometers operating at 600, 800, 900, and 950 MHz for ^{1}H. A detailed list of experiments used for backbone and side-chain assignments are provided in the Supplementary Material, along with details about relaxation and $^{1}D_{HN}$ residual dipolar coupling measurements.

NOE restraints were generated from ^{13}C-separated NOESY-HSQC and ^{15}N-separated NOESY-TROSY spectra, both of which used 100 ms mixing times, and a ^{13}C-separated NOESY-HMQC spectrum of the aromatic region with a 70 ms mixing time. Interchain restraints were generated by collecting a ^{13}C/^{15}N-filtered, ^{13}C-separated NOESY-HSQC spectrum with a 120 ms mixing time using a sample containing equimolar amounts of ^{13}C/^{15}N-labeled and unlabeled Swa_{DIMER}. This mixed sample was constituted in the presence of 4 M urea, refolded by dialysis into NMR buffer, and then concentrated to 0.8 mM prior to the ^{13}C/^{15}N-filtered NMR experiment.

NMR data were processed using a combination of TopSpin 3.7 (Bruker BioSpin) and NMRPipe.[32] Peak assignment and relaxation analysis were performed using CCPN Analysis 2.5.[33]

5.1 | Structure calculations

For calculating the structure of Swa_{DIMER}, we used chemical shift-matched peak lists from the NOESY spectra along with torsion angle restraints derived using TALOS-N[34] and $^{1}D_{HN}$ values for rigid parts of the protein (i.e., residues 208–268) as input for ARIA 2.3[27] (see Table 1). Many of the errors for torsion angle restraints calculated using TALOS-N were unusually small (between ±6° and ± 13°), so they were set to a minimum value of ±20°. The absence of peak doubling in the NMR spectra indicated that Swa_{DIMER} forms a symmetrical homodimer, so we included non-crystallographic symmetry (NCS) restraints in the structure calculation. We deviated from the standard ARIA protocol by increasing the number of cooling steps for the first and second simulated annealing periods (cool1 and cool2) by a factor of four and by calculating 30 structures (rather than 20) for each iteration. In the final iteration, 100 structures were calculated. The 20 structures with the lowest energy were selected for water refinement and used to generate the structural ensemble. Statistics describing the restraints used for the calculations and the resulting ensemble are provided in Table 1. Chemical shifts and restraints were deposited at the BioMagResBank (BMRB ID 30768) and atomic coordinates were deposited in the Worldwide Protein Data Bank (PDB ID 6XOR).

ACKNOWLEDGEMENTS

We thank Frank Löhr (Goethe-University Frankfurt) for his assistance in collecting the spectra for this study on instruments supported by the Research Infrastructure Activity in the seventh Framework Programme of the EC (Project 261863, Bio-NMR). The Oregon State University NMR Facility is funded in part by the National Institutes of Health (HEI Grant 1S10OD018518) and by the M. J. Murdock Charitable Trust (Grant 2014162). Nikolaus M. Loening was supported by the National Science Foundation (1617019 Amendment No. 1). Elisar Barbar acknowledges support from the National Science Foundation (Award 1617019).

AUTHOR CONTRIBUTIONS

Nikolaus Loening: Conceptualization; data curation; formal analysis; funding acquisition; investigation; validation; writing-original draft; writing-review and editing. **Elisar Barbar:** Conceptualization; data curation; formal analysis; funding acquisition; investigation; validation; writing-original draft; writing-review and editing.

ORCID

Nikolaus M. Loening https://orcid.org/0000-0002-5074-6906
Elisar Barbar https://orcid.org/0000-0003-4892-5259

REFERENCES

1. Anon. UniProt: a worldwide hub of protein knowledge. Nucleic Acids Res. 2019;47:D506–D515.
2. Schnorrer F, Bohmann K, Nüsslein-Volhard C. The molecular motor dynein is involved in targeting swallow and bicoid RNA to the anterior pole of drosophila oocytes. Nat Cell Biol. 2000;2:185–190.
3. Meng J, Stephenson EC. Oocyte and embryonic cytoskeletal defects caused by mutations in the drosophila swallow gene. Dev Genes Evol. 2002;212:239–247.
4. Wang L, Hare M, Hays TS, Barbar E. Dynein light chain LC8 promotes assembly of the coiled-coil domain of swallow protein. Biochemistry. 2004;43:4611–4620.
5. Kidane AI, Song Y, Nyarko A, et al. Structural features of LC8-induced self-association of swallow. Biochemistry. 2013;52:6011–6020.
6. Barbar E. Dynein light chain LC8 is a dimerization hub essential in diverse protein networks. Biochemistry. 2008;47:503–508.
7. Barbar E, Nyarko A. NMR characterization of self-association domains promoted by interactions with LC8 hub protein. Comput Struct Biotechnol J. 2014;9:e201402003.
8. Clark SA, Jespersen N, Woodward C, Barbar E. Multivalent IDP assemblies: Unique properties of LC8-associated, IDP duplex scaffolds. FEBS Lett. 2015;589:2543–2551.
9. Berman HM, Westbrook J, Feng Z, et al. The Protein Data Bank. Nucleic Acids Res. 2000;28:235–242.
10. Wang Y, Boudreaux DM, Estrada DF, Egan CW, St Jeor SC, De Guzman RN. NMR structure of the N-terminal coiled coil domain of the Andes hantavirus nucleocapsid protein. J Biol Chem. 2008;283:28297–28304.
11. Kobashigawa Y, Kumeta H, Kanoh D, Inagaki F. The NMR structure of the TC10- and Cdc42-interacting domain of CIP4. J Biomol NMR. 2009;44:113–118.
12. Junius FK, O'Donoghue SI, Nilges M, Weiss AS, King GF. High resolution NMR solution structure of the leucine zipper domain of the c-Jun homodimer. J Biol Chem. 1996;271:13663–13667.
13. MacKay JP, Shaw GL, King GF. Backbone dynamics of the c-Jun leucine zipper: ^{15}N NMR relaxation studies. Biochemistry. 1996;35:4867–4877.
14. Dames SA, Schönichen A, Schulte A, et al. Structure of the cyclin T binding domain of Hexim1 and molecular basis for its recognition of P-TEFb. Proc Natl Acad Sci U S A. 2007;104:14312–14317.
15. Kaplan AR, Brady MR, Maciejewski MW, Kammerer RA, Alexandrescu AT. Nuclear magnetic resonance structures of GCN4p are largely conserved when ion pairs are disrupted at acidic pH but show a relaxation of the coiled coil superhelix. Biochemistry. 2017;56:1604–1619.
16. Holliday MJ, Witt A, Rodríguez Gama A, et al. Structures of autoinhibited and polymerized forms of CARD9 reveal mechanisms of CARD9 and CARD11 activation. Nat Commun. 2019;10:3070.
17. Gordon-Smith DJ, Carbajo RJ, Yang JC, et al. Solution structure of a C-terminal coiled-coil domain from bovine IF(1): The inhibitor protein of F(1) ATPase. J Mol Biol. 2001;308:325–339.
18. Lu Q, Ye F, Wei Z, Wen Z, Zhang M. Antiparallel coiled-coil-mediated dimerization of myosin X. Proc Natl Acad Sci U S A. 2012;109:17388–17393.
19. Vavra KC, Xia Y, Rock RS. Competition between coiled-coil structures and the impact on myosin-10 bundle selection. Biophys J. 2016;110:2517–2527.
20. Song F, Li M, Liu G, et al. Antiparallel coiled-coil interactions mediate the homodimerization of the DNA damage-repair protein PALB2. Biochemistry. 2018;57:6581–6591.
21. Lavigne P, Crump MP, Gagné SM, Hodges RS, Kay CM, Sykes BD. Insights into the mechanism of heterodimerization from the 1H-NMR solution structure of the c-Myc-max heterodimeric leucine zipper. J Mol Biol. 1998;281:165–181.
22. Stathopulos PB, Schindl R, Fahrner M, et al. STIM1/Orai1 coiled-coil interplay in the regulation of store-operated calcium entry. Nat Commun. 2013;4:2963.
23. Hakansson-McReynolds S, Jiang S, Rong L, Caffrey M. Solution structure of the severe acute respiratory syndrome-coronavirus heptad repeat 2 domain in the prefusion state. J Biol Chem. 2006;281:11965–11971.
24. Stewart KD, Huth JR, Ng TI, et al. Non-peptide entry inhibitors of HIV-1 that target the gp41 coiled coil pocket. Bioorg Med Chem Lett. 2010;20:612–617.
25. Kühn J, Wong LE, Pirkuliyeva S, et al. The adaptor protein CIN85 assembles intracellular signaling clusters for B cell activation. Sci Signal. 2016;9:ra66.
26. Chen Z, Boyken SE, Jia M, et al. Programmable design of orthogonal protein heterodimers. Nature. 2019;565:106–111.
27. Rieping W, Habeck M, Bardiaux B, Bernard A, Malliavin TE, Nilges M. ARIA2: Automated NOE assignment and data integration in NMR structure calculation. Bioinformatics. 2007;23:381–382.

28. Crick FHC. The packing of α-helices: Simple coiled-coils. Acta Crystallogr. 1953;6:689–697.
29. Walshaw J, Woolfson DN. Socket: A program for identifying and analysing coiled-coil motifs within protein structures. J Mol Biol. 2001;307:1427–1450.
30. Grigoryan G, DeGrado WF. Probing designability via a generalized model of helical bundle geometry. J Mol Biol. 2011;405:1079–1100.
31. Bloyet L-M, Schramm A, Lazert C, et al. Regulation of measles virus gene expression by P protein coiled-coil properties. Sci Adv. 2019;5:eaaw3702.
32. Delaglio F, Grzesiek S, Vuister GW, Zhu G, Pfeifer J, Bax A. NMRPipe: A multidimensional spectral processing system based on UNIX pipes. J Biomol NMR. 1995;6:277–293.
33. Vranken WF, Boucher W, Stevens TJ, et al. The CCPN data model for NMR spectroscopy: Development of a software pipeline. Proteins. 2005;59:687–696.
34. Shen Y, Bax A. Protein backbone and sidechain torsion angles predicted from NMR chemical shifts using artificial neural networks. J Biomol NMR. 2013;56:227–241.
35. Laskowski RA, Rullmannn JA, MacArthur MW, Kaptein R, Thornton JM. AQUA and PROCHECK-NMR: Programs for checking the quality of protein structures solved by NMR. J Biomol NMR. 1996;8:477–486.
36. Chen VB, Arendall WB, Headd JJ, et al. MolProbity: All-atom structure validation for macromolecular crystallography. Acta Cryst D. 2010;66:12–21.
37. Pymol DW. An open-source molecular graphics tool. CCP4 Newsl. Protein Cryst. 2002;40:82–92.
38. Grigoryan G, Keating AE. Structural specificity in coiled-coil interactions. Curr Opin Struct Biol. 2008;18:477–483.

SUPPORTING INFORMATION

Additional supporting information may be found online in the Supporting Information section at the end of this article.

How to cite this article: Loening NM, Barbar E. Structural characterization of the self-association domain of swallow. *Protein Science*. 2021;30:1056–1063. https://doi.org/10.1002/pro.4055